Journal of Sound and Vibration (1999) **277**(3), 511–522
Article No. jsvi.1999.2296, available online at http://www.idealibrary.com on IDEAL®

NUMERICAL SIMULATION OF SELF-EXCITED THERMOACOUSTIC INSTABILITIES IN A RIJKE TUBE

C.-C. HANTSCHK AND D. VORTMEYER

Faculty of Mechanical Engineering, Technische Universität München, Boltzmannstrasse 15, *D*-85747 *Garching, Germany*

(*Received* 25 *August* 1998, *and in final form* 29 *March* 1999)

Self-excited thermoacoustic instabilities or oscillations occur in confined geometries and result from a feedback loop between the heat transferred to the fluid from a heat source and the acoustics of the geometry. If the heat input is at times of high pressure, a self-amplification of acoustic fluctuations may lead to high pressure amplitudes. The effect can be observed in a Rijke tube, a straight tube with a heating element made from hot wires or gauze that provides the heat input. In the presence of a gas flow, pressure oscillations are excited at one of the tube's natural frequencies. Two different kinds of Rijke tubes are modelled by using a control volume based finite difference method to solve iteratively the unsteady conservation equations for mass, momentum and energy. The obtained results are in good agreement with experiments. Besides the general behaviour of the oscillating system, non-linear effects are also accounted for by the simulations. The non-linearities in the heat transferred to the fluid from the heat source were investigated. These determine the limit cycle amplitudes of the self-excited oscillations.

1. INTRODUCTION

Self-excited thermoacoustic oscillations in confined geometries originate from an unsteady interaction and a feedback loop between flow, heat input, and the acoustics of the system. Lord Rayleigh stated already in 1877 that oscillations are most strongly excited if the fluctuations of the heat flux are in phase with the fluctuations of the pressure [1]. However, oscillations can also be obtained if the phase shift between the oscillations of heat flux and pressure is less than $\pm 90^\circ$ [2]. From the onset of the oscillations, the amplitudes grow until they reach a maximum, called the "limit cycle".

The energy supply for self-excited thermoacoustic oscillations can be provided by different ways of heat input, for example an exothermal chemical reaction in a combustion chamber. Overviews of such self-excited combustion instabilities or pulse combustion, are given in references [2–10]. The heat input can also originate from other sources such as hot wires or hot gauzes in the flow. An example for thermoacoustic oscillations caused by the unsteady heat flux from a hot gauze is the Rijke tube [11]. It is a straight tube with the heated gauze placed inside the tube.

0022-460X/99/430511 + 12 $30.00/0

Air flows through the tube and heats up when passing the gauze. Depending on the position of the gauze, its temperature, the acoustic boundary conditions of the tube and the flow velocity, pressure oscillations with amplitudes of several hundred Pa at one of the tube's natural frequencies can be observed. Contributions to the Rijke tube and related phenomena can be found, for example, in references [1, 12–19].

The limit cycle amplitude is mainly determined by non-linear effects and thus cannot be predicted by linear theory. The non-linear effects in a Rijke tube have been thoroughly investigated by Heckl in reference [20], where an empirical model is also developed for the prediction of the limit cycle amplitudes. A non-linear theory to predict the limit cycle of acoustic oscillations in combustion systems is presented in a recent work by Dowling [21]. The method is based on the assumption of a non-linear heat release rate of the flame and can also be applied to systems with other kinds of heat input. Analytical methods for the determination of limit cycle amplitudes that take the involved non-linearities into account are also given by Wicker *et al.* [22] and Margolis [23]. Various other important contributions have been made concerning non-linear effects in the thermoacoustic oscillations and the existence of limit cycles (see, for example, references [24–28]).

This paper presents the numerical simulation of non-linear self-excited thermoacoustic oscillations in two different types of a Rijke tube with a state-of-the-art CFD code. The time-dependent evolution of the oscillations until arriving at the limit cycle was modelled by solving the unsteady compressible Navier–Stokes equations together with the conservation equations for mass and energy and appropriate boundary conditions. These equations comprise all relevant effects influencing the oscillations, such as acoustics, flow, temperature distribution and the distributed region of heat input. It has been shown by Dowling [29] that all these parameters must be included in a model to describe thermoacoustic oscillations adequately. The flow was assumed to be two-dimensional, axisymmetric and laminar.

2. GENERAL MODELLING FEATURES

All simulations were performed by using the general purpose CFD code Fluent 4.4.4® that employs a control volume based finite difference method to solve the unsteady conservation equations for mass, momentum and energy. These are as follows: conservation of mass,

$$\frac{\partial \rho}{\partial t} + \frac{\partial (\rho u_i)}{\partial x_i} = 0, \tag{1}$$

conservation of momentum,

$$\frac{\partial (\rho u_j)}{\partial t} + \frac{\partial (\rho u_j u_i)}{\partial x_i} = -\frac{\partial p}{\partial x_j} + \frac{\partial \tau_{ji}}{\partial x_i}, \tag{2}$$

where

$$\tau_{ji} = \eta \left(\frac{\partial u_j}{\partial x_i} + \frac{\partial u_i}{\partial x_j} \right) - \frac{2}{3} \eta \frac{\partial u_k}{\partial x_k} \delta_{ji}, \tag{3}$$

conservation of energy,

$$c_p \frac{\partial(\rho T)}{\partial t} + c_p \frac{\partial(\rho u_i T)}{\partial x_i} - \frac{1}{\rho}\left(\frac{\partial(\rho p)}{\partial t} + \frac{\partial(\rho u_i p)}{\partial x_i}\right) = \frac{\partial}{\partial x_i}\left(\lambda \frac{\partial T}{\partial x_i}\right) + \tau_{ji}\frac{\partial u_j}{\partial x_i}. \quad (4)$$

These equations and the equation of state for an ideal gas

$$p/\rho = (\Re/W)\,T \quad (5)$$

comprise all important thermoacoustic effects which occur in the Rijke tube (nomenclature given in Appendix A).

Equations (1)–(5) were solved iteratively for a laminar, two-dimensional, and axisymmetric flow with structured, body-fitted computational grids. The heating element is designed as a series of heater bands with an assigned surface temperature. Figure 1 shows one of the modelled heating elements together with an example of a computational grid in the region of the element. The outer wall of the tube is set to be adiabatic. A zero velocity boundary condition was used for all surfaces.

Two different kinds of Rijke tube were modelled, one with both ends open and the other one having one end closed by a porous sintered metal plate. This plate was assumed to produce an acoustically closed boundary condition.

3. SIMULATION OF A RIJKE TUBE WITH AN OPEN–OPEN BOUNDARY

The geometry of the tube is shown in Figure 1. The tube is 3 m long ($= L$) and 0·1 m in diameter, the heating element is located 0·75 m ($= L/4$) away from the inlet cross-section. This type of Rijke tube has two acoustically open boundary conditions. The pressure at 0·1 m outside of the inlet and outlet cross-section (see Figure 1) was therefore assumed to be constant [30] and was set to $p_0 = 101\,325$ Pa at the outlet and to $p = p_0 + 0{\cdot}5$ Pa at the inlet. Under steady state conditions this pressure difference produces a gas flow with a mean velocity of 0·36 m/s through the tube at 293 K that decreases to 0·007 m/s when the limit cycle is reached.

The molecular weight W, the specific heat c_p and the viscosity η of the fluid were those of air at 273 K. The thermal conductivity was chosen ten times higher, $\lambda = 0{\cdot}2410$ W/(mK) in order to obtain a sufficient heat input from the heating element even though only four heater bands were present in the model. This enabled the use of a coarser computational grid and thus reduced the computational effort. The surface temperature of the heating bands was set and kept constant at 3000 K. Under steady conditions these assumptions lead to a temperature rise of the fluid from 293 to 807 K.

The heat flux $\dot{Q}_i$ from the heating band to a neighbouring fluid cell i is calculated from equation (6) with $T_{surface}$ as the temperature of the heater surface, $T_{cell\,centre}$ as the local fluid temperature in the centre of the fluid cell and $A_{surface}$ as the area of the contact surface. Δs is the distance between the cell centre and the hot surface:

$$\dot{Q}_i = \lambda \frac{T_{surface} - T_{cell\,centre}}{\Delta s} A_{surface}. \quad (6)$$

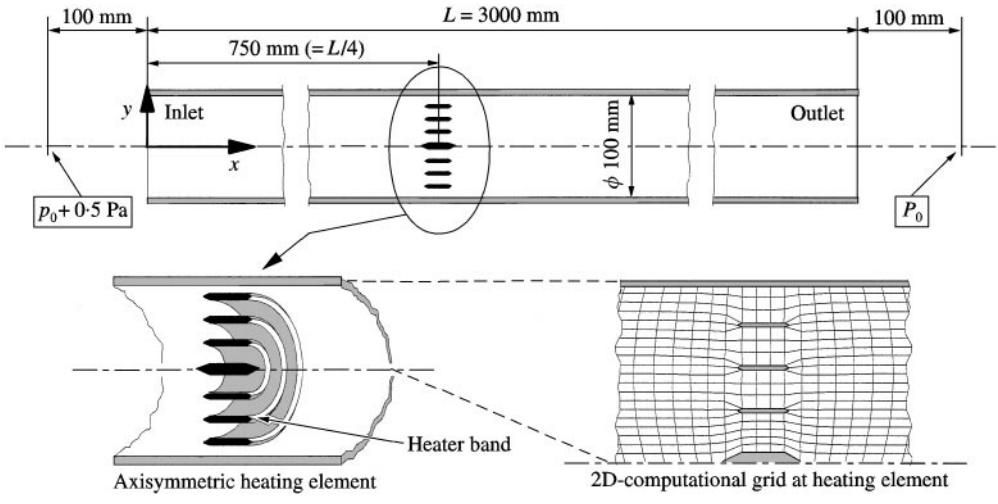

Figure 1. Geometry of the open–open Rijke tube with pressure boundary conditions. The heating element and the computational grid in the region of the element.

The total heat flux $\dot{Q}$ from the heating element to the gas stream results from a summation of all $\dot{Q}_i$:

$$\dot{Q} = \sum_i \dot{Q}_i. \tag{7}$$

If a small pressure disturbance ($\Delta p = 30$ Pa) is imposed on the obtained steady state solution the system becomes unstable and self-excited thermoacoustic oscillations evolve. Figure 2 shows the calculated pressure at the location of the heating element ($x = 0{\cdot}75$ m) after the onset of the oscillations and for the limit cycle.

The frequency of the estimated oscillations of 76 Hz corresponds to the first fundamental frequency of the heated open–open tube. The mode of the standing wave is shown in Figure 3. It is observed that the mode is "stretched" downstream of the heating element. This is due to the elevated temperature of 807 K in the hot part of the tube which in turn causes a higher speed of sound and therefore a longer wavelength of the standing acoustic wave.

The calculated pressure oscillations $\tilde{p}$ and the oscillating axial flow velocity u at the location of the heating element are shown in Figure 4(a), for the limit cycle. It can be seen that the velocity oscillations precede the pressure oscillations by about 90° in phase, as to be expected for the excited standing wave. The velocity oscillations lead to an oscillating heat flux $\dot{Q}$ transferred to the fluid from the heating element which is shown in Figure 4(b). Due to thermal inertia the maximum heat flux does not coincide with the maximum velocity but occurs with a certain time lag [31]. In Figure 4(b) the calculated pressure oscillations are also shown. It is observed that the maxima of the heat flux and pressure oscillation are close together (phase difference $\approx 35°$) thus meeting the requirement of the Rayleigh criterion.

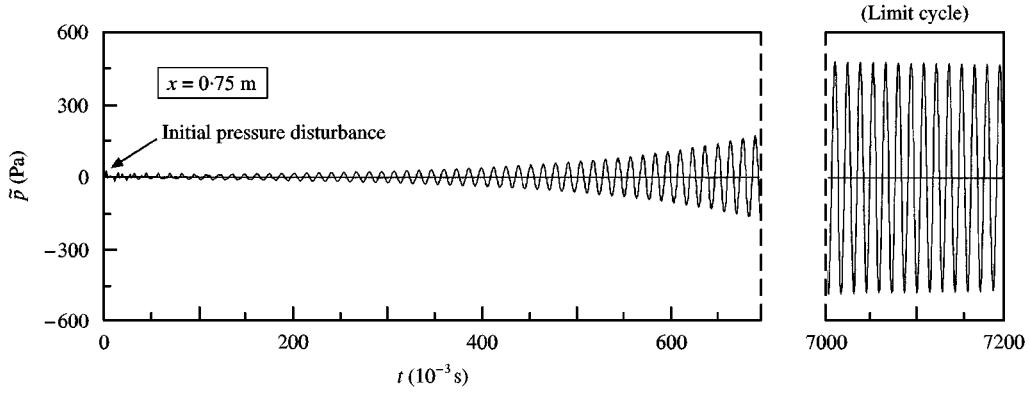

Figure 2. Evolution of self-excited pressure oscillations. Calculated pressure in the modelled open–open Rijke tube versus time, at the location of the heating element.

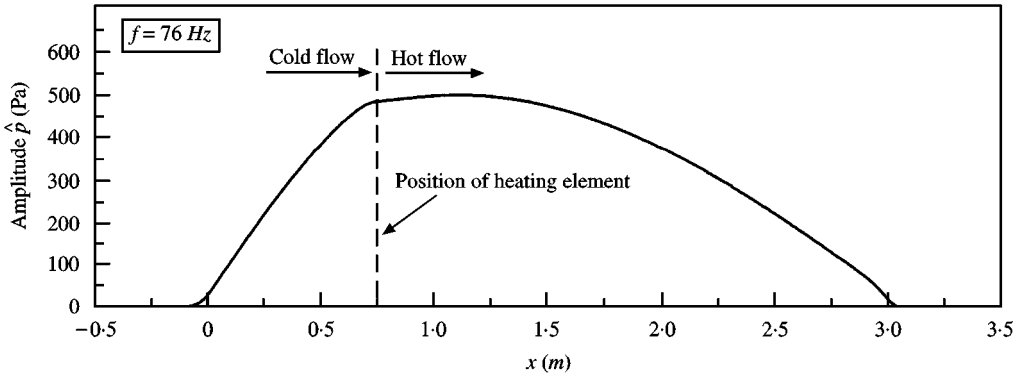

Figure 3. Under limit cycle conditions: computed pressure mode in the open–open Rijke tube.

Since the limit cycle amplitude of the velocity oscillation of 1·04 m/s is much larger than the average convective flow velocity of 0·12 m/s, it therefore produces considerable backflow ($u < 0$) at the heating element, once per cycle (see Figure 4(a)). This effect causes the non-harmonic shape of the heat flux oscillations in Figure 4(b) and is of importance for the amplitude limitation of the self-excitation process, as will be discussed later.

4. SIMULATION OF A RIJKE TUBE WITH A CLOSED–OPEN BOUNDARY AND COMPARISON WITH THE EXPERIMENTAL WORK

The second Rijke tube is of the acoustically closed–open boundary type with the heating element placed at $x = \frac{1}{2}L$. An arrangement of this kind was thoroughly investigated experimentally by Kunz [32] who, instead of a tube, used a duct of 0·989 m length ($= L$) and with a square cross-section of 0·028 m side length. The electric heater element which was placed at $x = 0{\cdot}495$ m ($= L/2$) consisted of 18 parallel flat wires (cross-section 0·2 mm × 1·75 mm, total length 0·504 m). The acoustically closed boundary condition was realized by a flat porous plate of

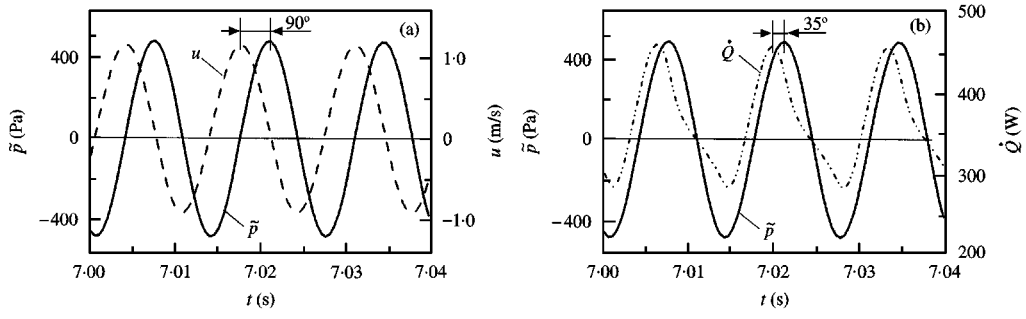

Figure 4. Calculated results for the open–open Rijke tube versus time for the limit cycle. (a) axial flow velocity u at the centre of the tube and pressure $\tilde{p}$, both at the position of the heating element; (b) pressure $\tilde{p}$ and total heat flux $\dot{Q}$ transferred from the heater wires to the fluid.

sintered material with an air stream flowing through it, at a constant velocity of 0·15 m/s.

The rectangular duct was modelled by an axisymmetric tube with the same cross-sectional area (diameter 0·0316 m). The parallel heater wires in the experimental set-up of Kunz were replaced in the model by concentric rings of flat wire with the same cross-section and total length. To obtain sufficient spatial resolution in the vicinity of the thin heater wires (thickness 0·2 mm) a very fine computational grid was used in this region. The constant inlet flow velocity of 0·15 m/s at the acoustically closed boundary condition agreed with that of the experimental arrangement. The boundary condition at the acoustically open end was set to a constant pressure at 0·032 m outside of the tube. In order to take into account the influence of temperature on the physical properties of air, the specific heat c_p, the viscosity η and the thermal conductivity λ were each modelled as temperature dependent [33]. At 273·15 K the following values apply: $c_p = 1006$ J/(kg K), $\eta = 1{\cdot}724 \times 10^{-5}$ kg/(m s) and $\lambda = 0{\cdot}0242$ W/(m K).

In his experimental work Kunz obtained an average heat flux of 54·5 W from the heating element to the air. The same heat flux was obtained in the simulation if the surface temperature of the heater wires was set to 745 K. This leads to the same temperature rise from 293 to 666 K (directly after the heating element) as in the experiments. The wall of the tube was assumed to be adiabatic. This assumption was not fulfilled by the experimental arrangement where wall heat losses were present.

Figure 5 shows the calculated pressure at the location of the heating element during the phase of the developing oscillations and for the limit cycle. Self-excited oscillations occur at a frequency of 297 Hz which is the frequency of the second harmonic of the heated tube. Oscillations of the same harmonic were observed in the experiments. The accompanying pressure mode is plotted in Figure 6. It is a three-quarter wave with a pressure node at the acoustically open boundary condition ($x = L$) and a pressure antinode at the acoustically closed boundary condition ($x = 0$). Due to the increased speed of sound in the hot section of the tube the mode is again stretched there.

Computed oscillations of axial flow, pressure and heat flux are shown in Figure 7 for the limit cycle. Figure 7(a) presents the axial velocity u in the centre of the tube

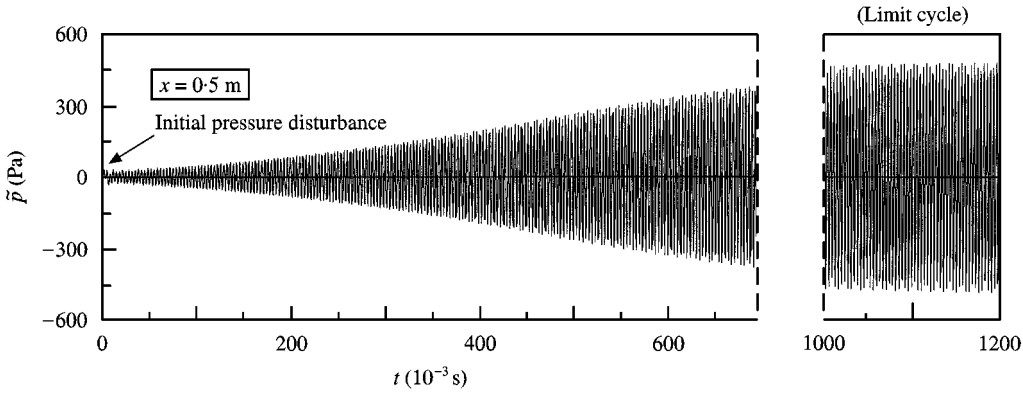

Figure 5. Evolution of self-excited pressure oscillations. Calculated pressure in the modelled closed–open Rijke tube versus time, at the location of the heating element.

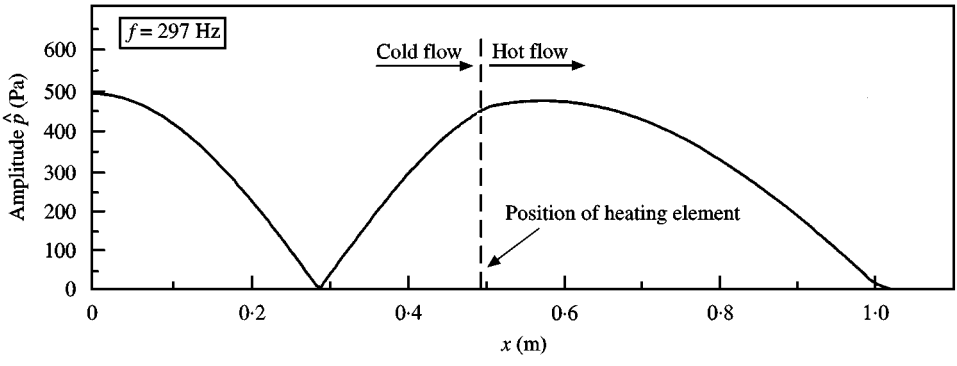

Figure 6. Calculated pressure mode in the closed–open Rijke tube under limit cycle conditions.

and the pressure $\tilde{p}$, both at the position of the heating element. Figure 7(b) shows $\tilde{p}$ together with the total heat flux $\dot{Q}$, which is transferred from the heater wires to the air. At this position it is observed that the pressure oscillations in Figure 7(a) lag the velocity oscillations by about 90° in phase and that the phase lag between the oscillations of pressure and heat flux in Figure 7(b) is about 25°. This means that the Rayleigh criterion is fulfilled as required. Figure 7(a) also exhibits a slight backflow ($u < 0$) at the heating element, once per cycle.

It is remarkable that in theory and from experiment only oscillations of the second harmonic are excited in the closed–open tube and not of the first harmonic, which cannot be excited because for this harmonic the pressure oscillations would precede the velocity oscillations at $x = \frac{1}{2}L$. Heat flux oscillations would be induced in an antiphase nature to the pressure oscillations. However, this is a stable situation according to the Rayleigh criterion. No oscillations are possible.

In Table 1 calculated and measured quantities are compared. It is found that the agreement for the oscillation frequencies and for the maximum values of the pressure and velocity amplitudes is quite satisfactory. The deviations originate from the fact, that the modelling assumptions did not quite match the experimental

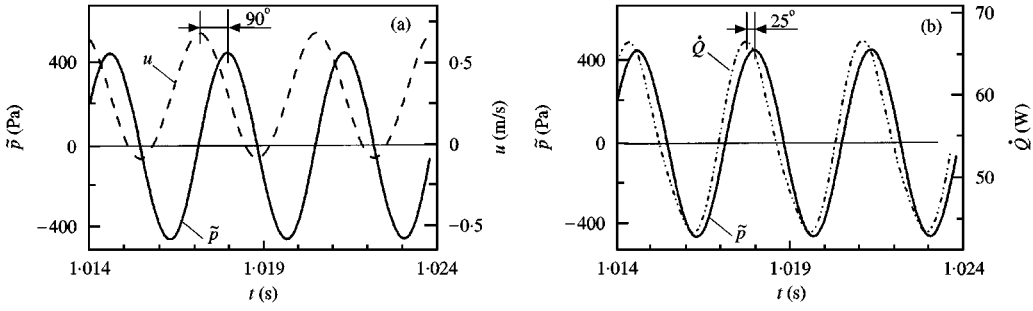

Figure 7. Calculated results for the closed–open Rijke tube versus time for the limit cycle. (a) axial flow velocity u at the centre of the tube and pressure $\tilde{p}$, both at the position of the heating element; (b) pressure $\tilde{p}$ and total heat flux $\dot{Q}$ transferred from the heater wires to the air.

TABLE 1

Comparison between simulation and experimental data

Value		Simulation	Experiment
Temperature	at inlet	293 K	293 K
	3 mm after heating element	666 K	665 K
Frequency		297 Hz	269 Hz
Heat losses to walls		0	Unknown
Max. pressure amplitude		496 Pa (148 dB)	450 Pa (147 dB)
Max. velocity amplitude		1·78 m/s	1·4 m/s

set-up. Instead of the adiabatic conditions as in the model, heat losses were present in the experiment. Therefore, while moving to the exit cross-section of the tube, the temperature of the hot air decreased considerably due to the wall heat losses. This results in a lower speed of sound, with the effect that indeed the experimentally determined frequencies should be lower than the calculated ones. The slight overprediction of the amplitudes may be due to differences in the acoustic boundary conditions of the model and the experiment. Dissipative energy losses within the sintered metal plate at the air inlet of the experiment are not taken into account by the model boundary condition. The initial experimental work was performed in 1981; unfortunately, at present it is not known how to improve the model.

5. NON-LINEARITIES AND AMPLITUDE LIMITATION

In agreement with the experimental work, the computations also predict a limit cycle with constant amplitudes of pressure, velocity and heat flux oscillations. Heckl [20] has studied in detail the effects which lead to the amplitude limitation and demonstrated that it is mainly caused by non-linearities in the heat flux from the heating element to the gas.

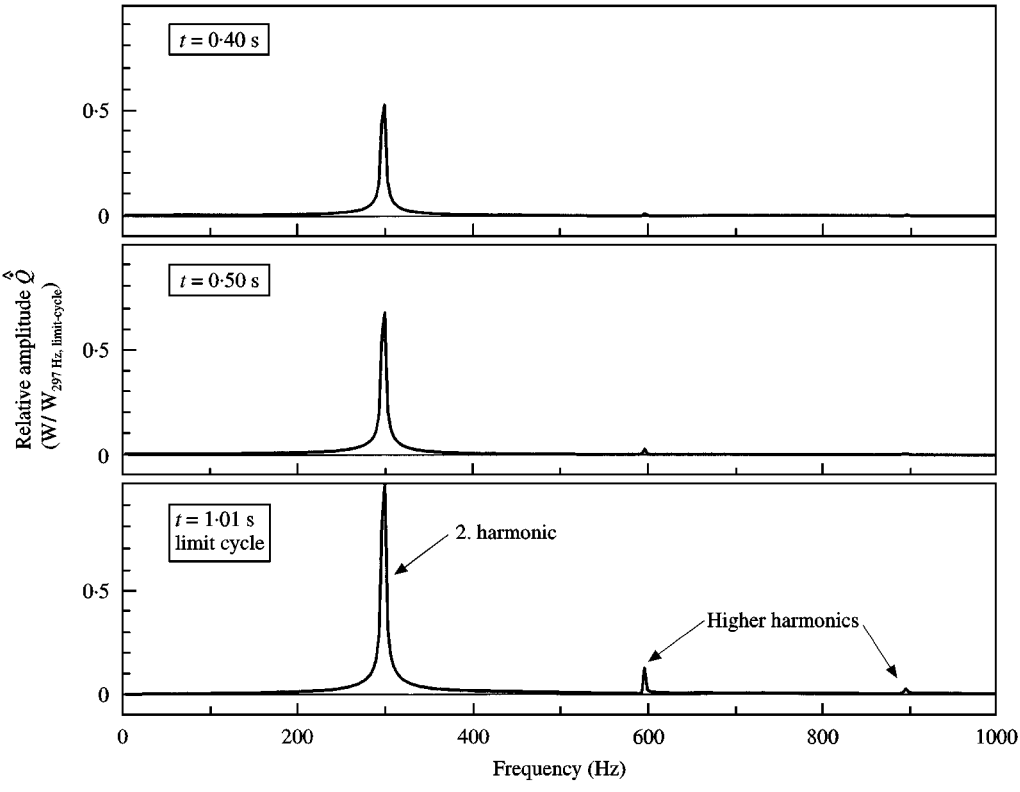

Figure 8. Frequency spectra of the calculated heat flux $\tilde{Q}$ at different times during the onset of oscillations and for the limit cycle.

This view is confirmed by the simulations. On following the increase of amplitudes from the onset of the oscillations, eventually a state is approached, where for short periods of time during each cycle, negative flow velocities are obtained (Figure 7(a)), causing a backflow of hot gas at the heating element. This effect imposes non-linearities on the oscillating heat flux with the result that higher harmonics appear in the frequency spectrum. This can be seen in Figure 8, where frequency spectra of the calculated heat flux $\tilde{Q}$ are shown at $t = 0{\cdot}40$ and $0{\cdot}50$ s, when amplitudes are still growing, and at $t = 1{\cdot}01$ s, when the limit cycle is reached. The amplitudes are scaled relative to the 297 Hz component at limit cycle. One can observe that components of higher harmonics (594 and 891 Hz) appear in the spectrum of the heat flux with growing amplitudes. These higher harmonics result entirely from non-linear effects and act like an external excitation on the corresponding higher harmonics of the pressure. This means that with increasing amplitudes an increasing amount of energy is fed into the higher harmonics with the effect that the energy fed into the 297 Hz oscillation is growing more slowly. The limit cycle is reached when the energy fed into the 297 Hz mode equals the energy losses due to viscous dissipation and radiation of sound.

Heckl [20] furthermore observed that the non-linearities in the heat flux already appeared when the velocity amplitudes $\hat{u}$ at the position of the heating gauze

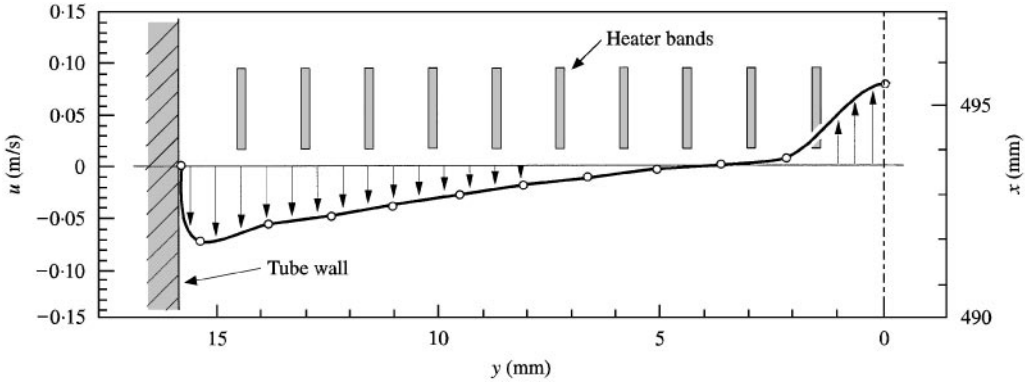

Figure 9. Calculated axial flow velocity distribution over y at 1·25 mm upstream of the heating element, while $\hat{u} = 0{\cdot}7\bar{u}$, and at the time during a cycle when the minimum velocity in the tube centre is reached.

amounted to only one third of the mean velocity $\bar{u}$. This also corresponds to our simulation results where the non-linearities appear between $\hat{u} \approx 0{\cdot}3 \cdot \bar{u}$ and $\hat{u} \approx 0{\cdot}5 \cdot \bar{u}$ with $\hat{u}$ and $\bar{u}$ taken in the tube centre (radial co-ordinate $y = 0$). This effect is explained by means of Figure 9, where the calculated axial flow velocity distribution is plotted versus y, at 1·25 mm upstream of the heating element. The profile is shown for $\hat{u} = 0{\cdot}7 \cdot \bar{u}$ and at the time during a cycle when the minimum velocity in the tube centre is reached. It is seen that while this velocity minimum is still positive, flow reversal already takes place in the region between $y \approx 3{\cdot}5$ mm and the tube wall, thus causing the non-linearities in the heat flux.

6. CONCLUSIONS

Self-excited thermoacoustic oscillations in a Rijke tube, that result from an interaction between the heat transferred to the fluid from hot wires and the acoustics in the geometry, were simulated successfully by solving the unsteady conservation equations for mass, momentum and energy together with the ideal gas equation and the boundary conditions. The applied code, Fluent 4.4.4®, is a commercially available control volume based CFD code that uses a finite difference method to solve the system of partial differential equations. In agreement with other work in the literature we find that self-excited oscillations are only to be obtained if the Rayleigh criterion is fulfilled and that the limit cycle amplitude is mainly determined by non-linearities in the heat flux from the heating element to the flow. Good agreement was obtained between simulation and experimental results.

REFERENCES

1. Lord Rayleigh 1877 *The Theory of Sound*, New York: Dover, 1945 re-issue. **2**, 226.
2. A. A. Putnam and W. R. Dennis 1954 *Journal of the Acoustical Society of America* **26**(5), 716–725. Burner oscillations of the gauze-tone type.
3. B. T. Zinn 1986 *Advanced Combustion Methods*. (Weinberg editor). London: Academic Press.
4. A. A. Putnam 1971 *Combustion Driven Oscillations in Industry*. New York: Elsevier.

5. F. E. C. Culick 1988 *AGARD-CP*-450. Combustion instabilities in liquid-fuelled propulsion systems — an overview.
6. S. M. Candel and T. J. Poinsot 1988 *Proceedings of the Institute of Acoustics* **10**, 103–153. Interactions between acoustics and combustion.
7. S. M. Candel 1992 24*th Symposium* (*Int.*) *on Combustion*, *The Combustion Institute*, 1277–1296. Combustion instabilities coupled by pressure waves and their active control.
8. B. T. Zinn 1992 24*th Symposium* (*Int.*) *on Combustion*, *The Combustion Institute*, 1297–1305. Pulse combustion: recent applications and research issues.
9. M. Barrère and F. A. Williams 1969 12*th Symposium* (*Int.*) *on Combustion*, *The Combustion Institute*, 169–181. Comparison of combustion instabilities found in various types of combustion chambers.
10. M. W. Thring 1969 12*th Symposium* (*Int.*) *on Combustion*, *The Combustion Institute*, 163–168. Combustion oscillations in industrial combustion chambers.
11. P. L. Rijke 1859 *Annalen der Physik* **107**, 339–343. Notiz über eine neue Art, die Luft in einer an beiden Enden offenen Röhre in Schwingungen zu versetzen.
12. G. F. Carrier 1955 *Quarterly of Applied Mathematics* **12**(4), 383–395. The mechanics of the Rijke tube.
13. J. L. Neuringer and G. E. Hudson 1952 *Journal of the Acoustical Society of America* **24**(6), 667–674. An investigation of sound vibrations in a tube containing a heat source.
14. C. Nicoli and P. Pelcé 1989 *Journal of Fluid Mechanics* **202**, 83–96. One-dimensional model for the Rijke tube.
15. A. A. Collyer and D. J. Ayres 1972 *Journal of Physics D: Applied Physics* **5**, L73–L75. The generation of sound in a Rijke tube using two heating coils.
16. M. A. Heckl 1988 *Journal of Sound and Vibration* **124**(1), 117–133. Active control of the noise from a Rijke tube.
17. J. A. Carvalho Jr., M. A. Ferreira, C. Bressan and J. L. G. Ferreira 1989 *Combustion and Flame* **76**, 17–27. Definition of heater location to drive maximum amplitude acoustic oscillations in a Rijke tube.
18. A. C. McIntosh and S. Rylands 1996 *Combustion Science and Technology* **113–114**, 273–289. A model of heat transfer in Rijke tube burners.
19. K. T. Feldman Jr. 1968 *Journal of Sound and Vibration* **7**(1), 83–89. Review of the literature on Rijke thermoacoustic phenomena.
20. M. A. Heckl 1990 *Acustica* **72**, 63–71. Non-linear acoustic effects in the Rijke Tube.
21. A. P. Dowling 1997 *Journal of Fluid Mechanics* **346**, 271–290. Nonlinear self-excited oscillations of a ducted flame.
22. J. M. Wicker, M. W. Yoon and V. Yang 1995 *Journal of Sound and Vibration* **184**(1), 141–171. Linear and non-linear pressure oscillations in baffled combustion chambers.
23. S. B. Margolis 1994 *Combustion and Flame* **99**, 311–322. The nonlinear dynamics of intrinsic acoustic oscillations in a model pulse combustor.
24. S. B. Margolis 1993 *Journal of Fluid Mechanics* **253**, 67–103. Nonlinear stability of combustion-driven acoustic oscillations in resonance tubes.
25. F. E. C. Culick 1971 *Combustion Science and Technology* **3**, 1–16. Non-linear growth and limiting amplitude of acoustic oscillations in combustion chambers.
26. F. E. C. Culick 1994 *AIAA Journal* **32**(1), 146–169. Some recent results for nonlinear acoustics in combustion chambers.
27. E. Awad and F. E. C. Culick 1986 *Combustion Science and Technology* **46**, 195–222. On the existence and stability of limit cycles for longitudinal acoustic modes in a combustion chamber.
28. J. D. Sterling 1993 *Combustion Science and Technology* **89**, 167–179. Nonlinear analysis and modelling of combustion instabilities in a laboratory combustor.
29. A. P. Dowling 1995 *Journal of Sound and Vibration* **180**(4), 557–581. The calculation of thermoacoustic oscillations.
30. A. P. Dowling and J. E. Ffowcs Williams 1983 *Sound and Sources of Sound*. Chichester: Ellis Horwood.

31. M. J. LIGHTHILL 1954 *Philosophical Transactions of the Royal Society of London A* **224**, 1–23. The response of laminar skin friction and heat transfer of fluctuations in the stream velocity.
32. W. KUNZ 1981 *Technische Universität München Dissertation.* Untersuchungen zum Anregungsmechanismus thermoakustischer Schwingungen am Beispiel des Rijke-Phänomens.
33. R. KRAUSS 1994 *VDI Wärmeatlas.* Düsseldorf: Verein Deutscher Ingenieure, seventh edition, Db16.

APPENDIX A: NOMENCLATURE

Symbols

A	area
c_p	specific heat
f	frequency
L	length
p	pressure
$\dot{Q}$	heat flux
s	distance
t	time
T	period $(1/f)$
T	temperature
u	axial velocity
u_i	ith velocity component
W	molecular weight
x	axial co-ordinate
x_i	ith spatial co-ordinate
y	radial co-ordinate
δ	Kronecker symbol
η	dynamic viscosity
λ	thermal conductivity
ρ	density
τ_{ij}	viscous stress tensor
∂	partial derivative
$\varnothing$	diameter

Superscripts

$\bar{}$	mean value
$\tilde{}$	oscillatory part
$\hat{}$	amplitude
. (dot)	time derivative

Subscripts

0	ambient state
i	ith component or summation index
j	jth component
k	kth component
n	nth harmonic
rel	relative (normalized) quantity

Constants

$\mathfrak{R}$	$= 8{\cdot}31451$ J/mol K universal gas constant